Journal of Nuclear Materials 493 (2017) 336–342

Contents lists available at ScienceDirect

Journal of Nuclear Materials

journal homepage: www.elsevier.com/locate/jnucmat

In situ micro-tensile testing on proton beam-irradiated stainless steel

H.T. Vo [a], A. Reichardt [a], D. Frazer [a], N. Bailey [a], P. Chou [b], P. Hosemann [a, *]

[a] Department of Nuclear Engineering, University of California, Berkeley, CA, USA
[b] Electric Power Research Institute, Palo Alto, CA, USA

HIGHLIGHTS

- *In situ* SEM micro-tensile testing on ion-beam irradiated materials.
- Micro-tensile yield stress and total elongation correlate well with macroscale tensile values.
- A force–displacement curve based analysis of slip localization is presented.

GRAPHICAL ABSTRACT

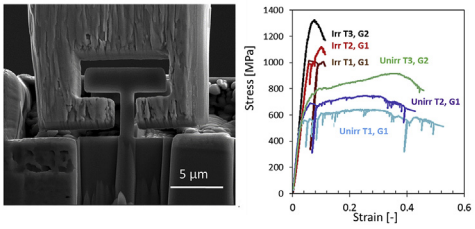

ARTICLE INFO

Article history:
Received 13 January 2017
Received in revised form
19 June 2017
Accepted 19 June 2017
Available online 21 June 2017

Keywords:
Radiation damage
Micro-tensile testing
Yield strength
Total elongation
Stainless steel
Localized deformation
Slip band

ABSTRACT

Small-scale mechanical testing techniques are currently being explored and developed for engineering applications. In particular, micro-tensile testing can add tremendous value, since the entire stress-strain curve, including the strain to failure, can be measured directly. In this work, 304 stainless steel specimens irradiated with 2 MeV protons to 10 dpa (full-cascade setting in the Stopping and Range of Ions in Matter, SRIM, software) at 360 °C was evaluated using micro-tensile testing. It was found that even on the micron scale, the measured strain corresponds well with macroscopic expectations. In addition, a new approach to analyzing sudden slip events is presented.

1. Introduction

Radiation damage in structural materials plays an important role in the reliability of existing nuclear reactors and deployment of new nuclear facilities. 304 stainless steel (304SS) is widely used for the core internal components of light-water reactors due to its resistance against aqueous corrosion and availability at the time of deployment [1]. However, in the harsh neutron-irradiated environment of LWRs, austenitic stainless steels experience microstructural and microchemical changes that increase susceptibility to stress corrosion cracking (SCC) and cause hardening, loss of ductility, and potentially void swelling [1–4]. A comprehensive understanding of how neutron irradiation affects the mechanical properties of austenitic stainless steels is important for the assessment of the reliability of reactors in long-term operation, which is associated with life extension.

Neutron irradiation, e.g. of stainless steel for the evaluation of yield strength over a range of doses [5], is lengthy and costly, especially for high doses. Therefore, ion-beam irradiation has been developed to mimic specific aspects of microstructural evolution

* Corresponding author. 4169 Etcheverry Hall, Berkeley, CA 94720, USA.
E-mail address: peterh@berkeley.edu (P. Hosemann).

http://dx.doi.org/10.1016/j.jnucmat.2017.06.026
0022-3115/

[6]. However, although it offers the advantages of high dose rate, little to no activation, and excellent control over the irradiation condition [6], the ion penetration depth is limited to the order of microns, which makes standard mechanical testing challenging. However, the advent of small-scale mechanical testing enables the measurement of ion-beam irradiated samples [7–9]. In previous work, *ex situ* nanoindentation and micropillar compression were performed over a range of temperatures on proton-irradiated 304SS [7,10] to characterize yield strength, hardness, and work-hardening. In this study, *in situ* SEM micro-tensile testing has been developed and deployed to measure the change in YS and total elongation (TE) due to irradiation damage. By testing a specimen *in situ*, the load-displacement curve can be correlated with the deformation process observed during testing [11–13]. Additionally, the effect of post-irradiation annealing is investigated.

2. Materials and methods

The composition of the 304 SS in this study is a standard-grade 304 that has the nominal wt.% composition of <0.08% C, 17.5–20% Cr, 8–11%, <2% Mn, <1% Si, <0.045% P, and <0.03% S. Two 304SS specimens were irradiated with protons to 10 dpa (flat displacement damage profile) at a dose rate of ~8×10^{-6} dpa/s and a temperature of 360° ± 10 °C by the Michigan Ion Beam Laboratory (MIBL) using a Tandetron accelerator. Fig. 1(a) displays the expected damage profile of the 2 MeV proton irradiation in the 304SS. Additional details of the irradiation procedure have been published in Ref. [14]. One of the two irradiated 304 SS samples was subsequently annealed at 500 °C for 1 h. From the isochronal annealing curve of the iron system, the vacancies complexes are mobile at the irradiation temperature of 360 °C [15]. The sample was annealed at 500 °C for 1 h post-irradiation to anneal out the irradiation damage (dislocation loops and defect clusters). The micro-tensile testing of the annealed samples were performed to observe the extent of the annealing.

The dose and dose rate were calculated using SRIM software [7]. The displacement energy used for the SRIM simulations is 40 eV. There are two options in SRIM for calculations of dose: “full cascade” and “Khinchin-Pease.” Unless otherwise specified, this study uses the full-cascade option in order to maintain consistency with a large number of prior publications across the years that use proton irradiation to investigate radiation damage. At the same time, a recent publication by Stoller et al. [16] establishes that the Khinchin-Pease option is more appropriate when comparing ion and neutron doses. The Khinchin-Pease (K-P) value is a factor of 2 less than the full-cascade value; that is, 10 dpa (full-cascade) corresponds to 5 dpa (K-P). Therefore, when this study compares the mechanical properties of proton-irradiated to neutron-irradiated stainless steels, the K-P dose values will be used and will be designated clearly by the suffix (K-P).

A FEI Quanta 3D FEG dual-beam FIB/SEM (with a focused gallium-69^{+} ion beam) was used to manufacture tensile bars, as shown in Fig. 1(b) and (c); their gauge length is ~4.5 μm and their cross-sectional area is ~1.3×1.3 μm. Rough milling was conducted at 30 keV with currents of 1–3 nA, and the final cleaning was performed at 0.3 nA.

Electron backscatter diffraction (EBSD) was used to map the grain and grain orientations of selected regions prior to sample fabrication, which allowed the tensile bars to be located within large single grains and allowed the determination of the Schmid factor of each grain along the axis of the tensile bars. Within a single grain, tensile bars were fabricated in both the flat displacement damage region of the irradiated zone within ~10 μm of the surface and the unirradiated region deeper than ~20 μm from the surface (Fig. 1(b)). Having samples within single grains allow the cleanest possible comparison between irradiated and unirradiated mechanical properties. Critical resolved shear stress is used for comparison among grains of different crystal orientations, because the Schmid factor of each grain has been used to account for the differences.

A customized tensile gripper assembly was designed, manufactured, and attached to the Hysitron PI-85 Picoindenter system; the gripper was fabricated from a tungsten needle mounted on a tip adapter for the indenter. The *in situ* PI-85 Picoindenter can apply load in tension and compression. Tension mode is selected in the Hysitron Pi-85 software for the micro-tensile testing. The tensile gripper adapter is used in place of a typical indenter tip, as shown in Fig. 1(b). Prior to testing, the sample was aligned and the gripper was placed in position, as shown in Fig. 1(d). The tests were conducted *in situ* in the SEM under displacement control at a rate of 10 nm/s, which is equivalent to a strain rate of ~2×10^{-3} s. The tensile bars were tested to failure. A video of each test was recorded. Three tensile bars were tested for each of three conditions: as-irradiated, post-irradiation annealed (PIA), and unirradiated.

Supplementary video related to this article can be found at http://dx.doi.org/10.1016/j.jnucmat.2017.06.026.

3. Experimental results

Engineering stress-strain curves were calculated from the load-displacement data from the indenter. Fig. 2(a) compares the stress-strain curves of the irradiated and unirradiated tensile bars; note that two irradiated and two non-irradiated tensile bars are located within Grain 1 (G1), and one irradiated and one unirradiated tensile bars are located within Grain 2 (G2). The yield strengths (YS) among irradiated and unirradiated tensile bars within one grain can be directly compared, but the YS from different grains cannot be. The critical resolved shear stress (CRSS) should be used for comparison among different grains. Fig. 2(b) compares the stress-strain curves of the irradiated and post-irradiation annealed (PIA) tensile bars. Because PIA was conducted on a separate proton-irradiated sample, the irradiated and PIA tensile bars are located on different samples and therefore in different grains. None of the irradiated YS values can be directly compared against the PIA YS values.[1] CRSS should be used for comparisons. The YS, CRSS, and total elongation (elastic strain and plastic strain) values are tabulated in Table 1. (The standard 0.2% offset YS are obtained from the stress-strain curves.) The average CRSS of the unirradiated, irradiated, and PIA samples are 213 MPa, 438 MPa, and 319 MPa, respectively; the corresponding average TEs are 47%, 11%, and 27%.

Images of the tensile bars strained to failure are shown in Fig. 3. Unirradiated tensile bars deformed via the formation of multiple slip steps occurring along certain slip planes. They also experienced work hardening after yield. In contrast, irradiated tensile bars failed suddenly at one slip plane, without the clear appearance of other slip events, consistent with their significantly lower average TE and higher average CRSS (11%, 438 MPa, respectively) relative to unirradiated tensile bars (47%, 213 MPa, respectively). Furthermore, they experienced work softening, rather than work hardening after yield. After annealing at 500 °C for 1 h, the ductility was partially recovered (Fig. 2(b)). Fig. 3(c) and (d) show that cracks formed at slip steps of the PIA tensile bars but became blunted; subsequent deformation occurred in a “tearing” fashion until failure.

[1] The Schmid factor of the grain in the PIA sample (0.408) was chosen to be similar to the Schmid factors of the grains in the as-irradiated sample (0.445 and 0.36), to minimize the adjustment for different crystal orientations.

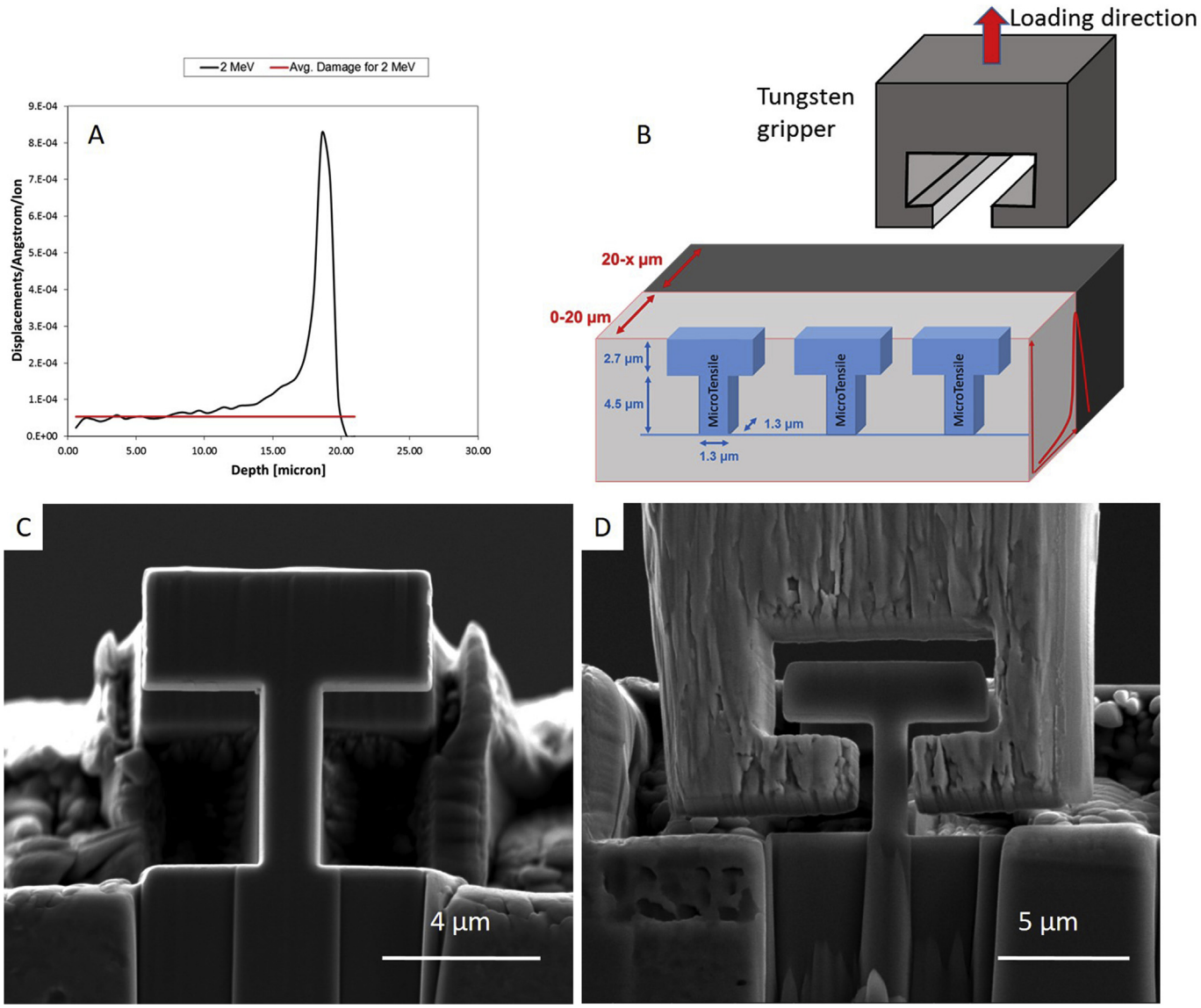

Fig. 1. (a) Dose profile obtained from full-cascade SRIM calculations. (b) Schematic of the tensile gripper and the sample; light grey represents the irradiated region and dark grey represents the unirradiated region. A representative plot of the dose profile is shown on the side of the rectangular volume. (c) Representative image of a micro-tensile bar. (d) Gripper in testing position.

4. Discussion

The micro-tensile results here are similar to macroscopic tensile test results in literature. Empirically modeled trend curves that represent the nominal behavior of austenitic stainless steels [17,18] neutron-irradiated at ~600 K and tested at room-temperature indicate that where the unirradiated YS is ~300 MPa, at 10 dpa, the irradiated YS is ~1000 MPa; and where the unirradiated TE is ~60%, the irradiated TE is ~20%. The dose of the proton-irradiated material of this study is only 5 dpa K-P. Since the irradiation-induced hardening saturates after a ~5 dpa neutron dose, similar change in YS should be observed at 5 dpa K-P and a 10 dpa neutron dose [19]. It is important to note that the data presented in this study is single-crystal data, while the macroscopic data were obtained from polycrystals; this difference is mitigated by the nanoscale nature of the radiation damage that causes the changes in mechanical properties. The good correlation is nonetheless remarkable.

The elastic moduli calculated from the stress-strain curves obtained here are ~30 GPa compared to expected elastic moduli of ~200 GPa. However, a comparison between the strain measured on the transducer and the strain measured via image correlation on the recorded movie conducted on a different material suggests that the difference originates from the system compliance. It has been found that a correction factor can be applied to correct for the compliance. However, the movies recorded do not have sufficient resolution, so this approach is not applied on the 304SS samples discussed here.

For unirradiated tensile bars, multiple load drops correlated to activation of the slip planes were observed on the stress-strain plots. In contrast, irradiated tensile bars experience one or a few severe slip events before failure (at significantly lower TE). The testing was performed in displacement-controlled mode, with set displacement and acquisition rates. Since the Hysitron indenter is a force-controlled system, the software implements a feedback loop between the applied load and the measured displacement; the

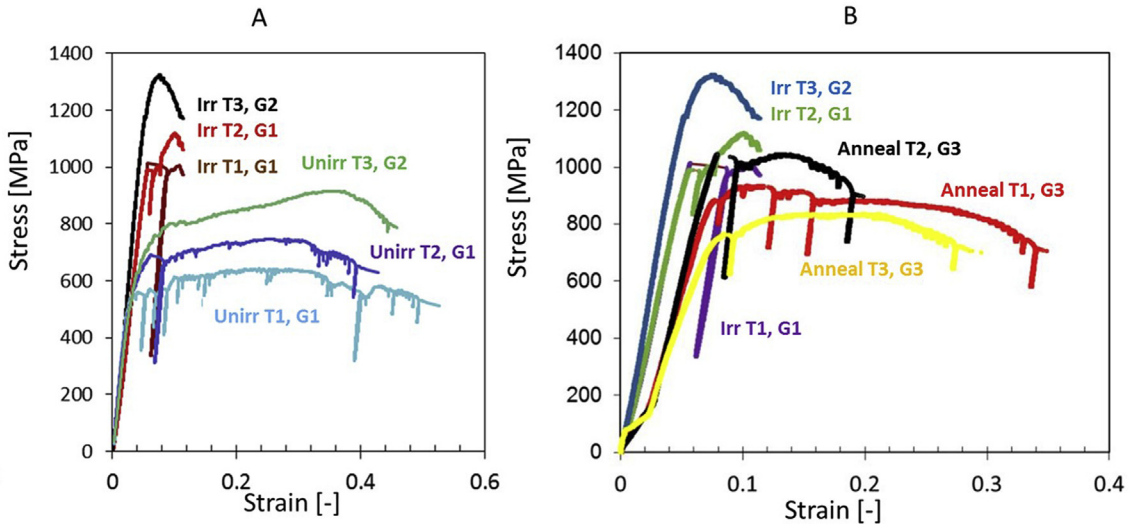

Fig. 2. (a) Stress-strain curves of unirradiated and as-irradiated tensile bars. (b) Stress strain curves of as-irradiated and post-irradiation-annealed (PIA) tensile bars.

Table 1
Detailed analysis of micro-tensile test data.

	Micro-tensile sample No.	Loading orientation	Max Schmid factor	0.2% offset YS [MPa]	CRSS [MPa]	% TE
Unirradiated	1	[113]	0.445	484	215	53
	2	[113]	0.445	505	225	43
	3	[223]	0.36	550	198	46
Irradiated	1	[113]	0.445	1012	450	11
	2	[113]	0.445	989	440	11
	3	[223]	0.36	1176	423	11
Post-irradiation annealed	1	[112]	0.408	832	340	34
	2	[112]	0.408	877	358	20
	3	[112]	0.408	639	260	28

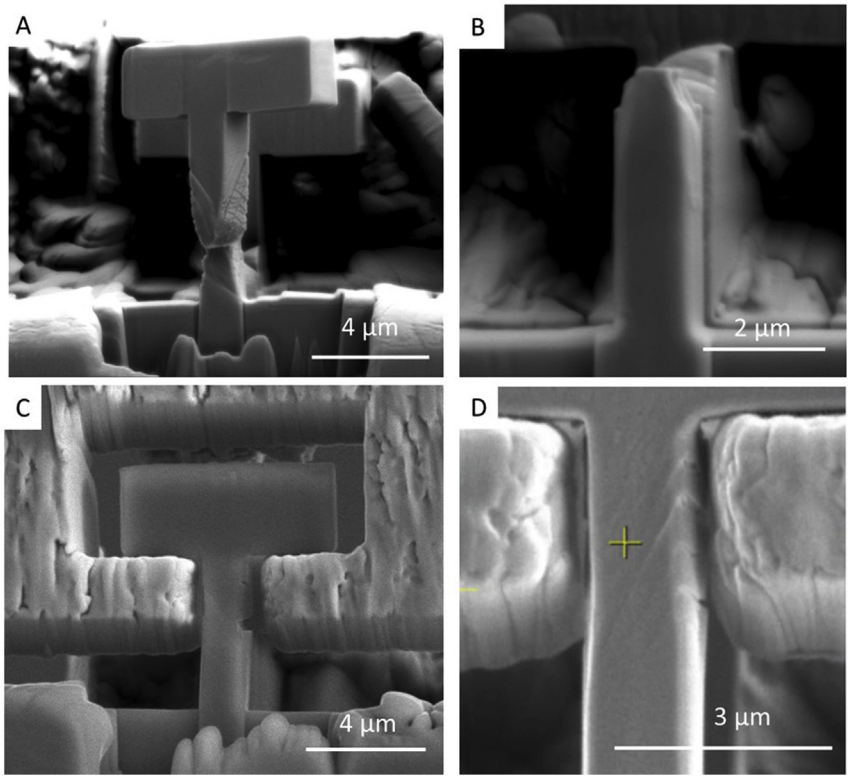

Fig. 3. Comparison of deformation behavior among micro-tensile tests. (a) Many slip bands and significant necking are observed in an unirradiated tensile bar. (b) Brittle fracture surface of an as-irradiated tensile bar. (c) and (d) "Tearing" behavior is observed in the post-irradiation-annealed (PIA) tensile bar; cracks form at the slip steps but are blunted.

applied load is continually adjusted to maintain the constant displacement rate. When the speed of the feedback loop is not sufficient to capture a sudden change in displacement, the applied load drops abruptly until the system catches up with the change in displacement. Consequently, one can quantify the slip events.

The number of load drops (sudden slip events) in the stress-strain curve can be counted. The start and end points of a load drop can be identified, and the area underneath the curve between those points represents the energy dissipated during the slip event. Since the slip events are caused by sudden dislocation motion, one can calculate the energy needed to move a dislocation through the pillar utilizing the Peierls stress. The Peierls stress is given by

$$\tau_{\downarrow} Peierls = \frac{2G}{1-\nu} * \exp\left(\frac{2\pi d}{(1-\nu)b}\right) \quad (1)$$

where G is the shear modulus, b is the burgers vector, ν is the Poisson's ratio and d is the interplanar spacing. The shear modulus of stainless steel in the (111) plane is 650 MPa [20]; the lattice constant is 0.351 nm [21], leading to a burgers vector of 0.248 nm and an interplanar spacing of 0.202 nm. Therefore, the Peierls stress is 118 MPa. The work a dislocation must perform in order to glide through the entire tensile bar can be calculated using:

$$W = \tau_{Peierls} * b * l * tl \quad (2)$$

where l is the dislocation line length (gage diameter), b is the burgers vector, and tl is the distance the dislocation traverses. If one assumes a nearly 45° slip plane, a 1.7 μm gage diameter translates to a 2.4 μm travel distance for the dislocation. The angle of the slip plane traces is assumed to be 45° for simplicity, since the SEM images during the testing were not captured for all tests. Also, the SEM images of the deformed micro-tensiles, such as Fig. 3(d), only provide a 2-D perspective of the slip plane traces, so the exact angles are not known. The energy required for a dislocation to travel through the tensile bar is then $1.2*10^{-13}$ Nm. Equation (2) can be expanded with account for the surface created by the slip step, with γ being the surface energy.

$$W = \tau_{Peierls} * b * l * tl + \gamma * b * l \quad (3)$$

The surface energies of 304SS stainless steel have not been determined, but the surface energies of pure nickel are reported based on modeling to be between 2.011 N/m and 2.368 N/m depending on the crystal orientation [22]. Therefore, surface energy contribution, $\sim 1*10^{-15}$ Nm, is insignificant compared to the contribution from the Peierls stress and can therefore be neglected.

The average number of dislocations per load drop (slip channel) traversing the tensile bar and the anticipated slip-step height can be determined from the average energy per load drop and the work required to move a dislocation ($1.2*10^{-13}$ Nm, as discussed earlier). The average energy per load drop can be calculated by assuming that all plastic deformation takes place within the individual slip channels and is therefore the total area under the load-displacement curve (not including the elastic part) divided by the total number of load drops. Fig. 4 shows the raw load-displacement curves of the unirradiated, irradiated, and post-irradiation-annealed tensile tests. Of course, this method neglects that fact that some load drops are more severe than others. However, we chose this method over an individual analysis since slow response

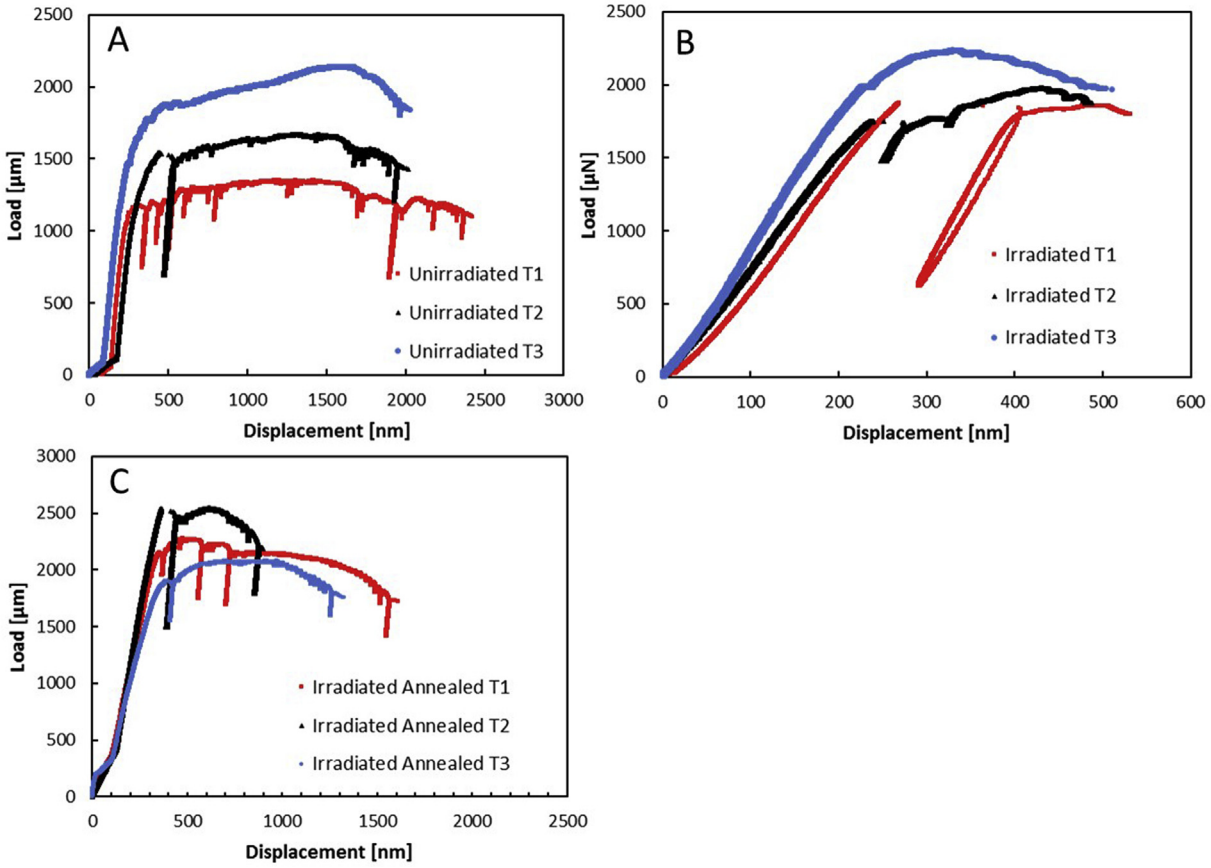

Fig. 4. The as-recorded load-displacement curves of the (a) unirradiated, (b) irradiated, (c) post-irradiation-annealed tensile tests.

Table 2
Slip behavior analysis of micro-tensile test data.

		Total Plastic Energy Released [10^{-9} Nm]	Number of Load Drops	Average Energy per Load Drops [10^{-10} Nm]	Number of Dislocations
Not irradiated	1	2.71	56	0.483	403
	2	2.55	37	0.689	574
	3	3.51	27	1.30	1083
Irradiated	1	0.486	1	4.86	4050
	2	0.463	2	2.32	1933
	3	0.608	1	6.08	5067
Irradiated and Annealed	1	2.63	34	0.773	644
	2	1.29	17	0.757	631
	3	1.86	20	0.929	774

of the load train may lead to an error for individual, more severe load drops and could make a comparison more difficult. Increased data acquisition rates may make future tests more precise, allowing individual load drop analysis.

Table 2 tabulates the average energy per load drop and the number of dislocations per load drop. A clear difference is observed. In unirradiated tensile bars, 400–1100 dislocations are associated with an average load drop, while in irradiated tensile bars, 1900–4100 dislocations are associated with an average load drop. The corresponding slip heights are 99–273 nm in the unirradiated tensile bars and 471–1017 nm in the irradiated tensile bars. Since the slip step heights are not precisely quantifiable, the considerations above are intended to provide a qualitative comparison.

The main strengthening features in stainless steels irradiated at light-water-reactor relevant temperatures are faulted Frank loops and small defect clusters [1,19]. The motion of initial dislocations through these nanoscale radiation-induced defects creates narrow defect-free channels that localize additional plastic deformation within them, leading to large strains within their small volumes [23]. Although no TEM was performed, the authors hypothesize that the highly-localized slip and large slip steps observed in the as-irradiated tensile bars arise from the formation of defect-free channels. After annealing at 500°C for 1 h, the CRSS of the specimens decreased and TE partially recovered, consistent with the expectation that the radiation-induced defects have been partially removed.

In Ref. [10], nanohardness of unirradiated and proton-irradiated 304 SS, from the same specimens as this study, were reported to be 3.23 ± 0.36 GPa and 5.58 ± 0.22 GPa. Various empirical relationships between hardness and yield strength have been established in the literature. Equations (4) and (5) are two such relationships that convert Vickers hardness to YS [24,25].

$$\sigma_y = 2.5(H_v - 68) \tag{4}$$

$$\sigma_y = 2.7H_v - 125 \tag{5}$$

The geometric relationship between the Berkovich nanoindenter and the Vicker's indenter was established in [26].

$$H_V = 0.0945H_{Berk} \tag{6}$$

Equation (4) calculates the unirradiated and irradiated YS values to be 330 and 1022 MPa, respectively. Similarly, Equation (5) calculates the unirradiated and irradiated YS values to be 415 and 1162 MPa, respectively. These calculated YS values correlate well with the micro-tensile measurements in Table 1. It is important to note that the indentations were not conducted in single grains of the same orientation. The discrepancies between the YS values obtained from micro-tensile and nanohardness measurements can be caused by sampling different grain-orientation grains.

5. Conclusion

This study applies quantitative micro-tensile testing on ion-beam-irradiated 304SS to increase the understanding of plastic deformation of irradiated stainless steel. Yield stress and critical resolved shear stress were measured and correlated well to literature values. Micro-tensile testing also enables the measurement of strain-to-failure, which is either not accessible or not easily accessible by other micromechanical techniques such as nano-indentation, micropillar compression, and micro-cantilever bending. The values of strain-to failure measured by (single-crystal) micro-tensile tests are in good agreement with macro-scale (polycrystal) tensile tests. A novel approach has been applied to quantify the average energy associated with a slip event and to estimate the number of dislocations participating in the slip event.

Acknowledgement

The authors thank the Electric Power Research Institute and the Nuclear Energy University Program for funding this research (Grant No. 13-5161). The authors thank the Biomolecular Nanotechnology Center (BNC) at the University of California, Berkeley for providing access to its FIB instrument. The authors thank AJ Gubser for manufacturing the tensile gripper.

References

[1] B.H. Sencer, G.M. Bond, M.L. Hamilton, F.A. Garner, S.A. Maloy, W.F. Sommer, Microstructural origins of radiation-induced changes in mechanical properties of 316 L and 304 L austenitic stainless steels irradiated with mixed spectra of high-energy protons and spallation neutrons, J. Nucl. Mater. 296 (2001) 112–118, http://dx.doi.org/10.1016/S0022-3115(01)00512-8.
[2] J.A. Sharon, K. Hattar, B.L. Boyce, L.N. Brewer, Compressive properties of ⟨110⟩ Cu micro-pillars after high-dose self-ion irradiation, Mater. Res. Lett. 2 (2014) 57–62, http://dx.doi.org/10.1080/21663831.2013.859179.
[3] M.D. McMurtrey, G.S. Was, L. Patrick, D. Farkas, Relationship between localized strain and irradiation assisted stress corrosion cracking in an austenitic alloy, Mater. Sci. Eng. A 528 (2011) 3730–3740, http://dx.doi.org/10.1016/j.msea.2011.01.073.
[4] B.D. Wirth, How does radiation damage materials? Science 318 (2007) 923–924, http://dx.doi.org/10.1126/science.1150394.
[5] M.L. Hamilton, F.A. Garner, M.B. Toloczko, S.A. Maloy, W.F. Sommer, M.R. James, P.D. Ferguson, M.R. Louthan Jr., Shear punch and tensile measurements of mechanical property changes induced in various austenitic alloys by high-energy mixed proton and neutron irradiation at low temperatures, J. Nucl. Mater. 283–287 (Part 1) (2000) 418–422, http://dx.doi.org/10.1016/S0022-3115(00)00363-9.
[6] G.S. Was, J.T. Busby, T. Allen, E.A. Kenik, A. Jensson, S.M. Bruemmer, J. Gan, A.D. Edwards, P.M. Scott, P.L. Andreson, Emulation of neutron irradiation effects with protons: validation of principle, J. Nucl. Mater. 300 (2002) 198–216, http://dx.doi.org/10.1016/S0022-3115(01)00751-6.
[7] H. Vo, A. Reichardt, C. Howard, M.D. Abad, D. Kaoumi, P. Chou, P. Hosemann, Small-scale mechanical testing on proton beam-irradiated 304 SS from room temperature to reactor operation temperature, JOM 67 (2015) 2959–2964, http://dx.doi.org/10.1007/s11837-015-1596-0.
[8] P. Hosemann, J.G. Swadener, D. Kiener, G.S. Was, S.A. Maloy, N. Li, An exploratory study to determine applicability of nano-hardness and micro-compression measurements for yield stress estimation, J. Nucl. Mater. 375

(2008) 135–143, http://dx.doi.org/10.1016/j.jnucmat.2007.11.004.
[9] D. Kiener, A.M. Minor, O. Anderoglu, Y. Wang, S.A. Maloy, P. Hosemann, Application of small-scale testing for investigation of ion-beam-irradiated materials, J. Mater. Res. 27 (2012) 2724–2736, http://dx.doi.org/10.1557/jmr.2012.303.
[10] A. Lupinacci, K. Chen, Y. Li, M. Kunz, Z. Jiao, G.S. Was, M.D. Abad, A.M. Minor, P. Hosemann, Characterization of ion beam irradiated 304 stainless steel utilizing nanoindentation and Laue microdiffraction, J. Nucl. Mater. 458 (2015) 70–76, http://dx.doi.org/10.1016/j.jnucmat.2014.11.050.
[11] A. Reichardt, M. Ionescu, J. Davis, L. Edwards, R.P. Harrison, P. Hosemann, D. Bhattacharyya, In situ micro tensile testing of He^{+2} ion irradiated and implanted single crystal nickel film, Acta Mater. 100 (2015) 147–154, http://dx.doi.org/10.1016/j.actamat.2015.08.028.
[12] P. Hosemann, D. Kiener, Y. Wang, S.A. Maloy, Issues to consider using nano indentation on shallow ion beam irradiated materials, J. Nucl. Mater. 425 (2012) 136–139, http://dx.doi.org/10.1016/j.jnucmat.2011.11.070.
[13] R. Kasada, Y. Takayama, K. Yabuuchi, A. Kimura, A new approach to evaluate irradiation hardening of ion-irradiated ferritic alloys by nano-indentation techniques, Fusion Eng. Des. 86 (2011) 2658–2661, http://dx.doi.org/10.1016/j.fusengdes.2011.03.073.
[14] G. Gupta, Z. Jiao, A.N. Ham, J.T. Busby, G.S. Was, Microstructural evolution of proton irradiated T91, J. Nucl. Mater. 351 (2006) 162–173, http://dx.doi.org/10.1016/j.jnucmat.2006.02.028.
[15] C.-C. Fu, J.D. Torre, F. Willaime, J.-L. Bocquet, A. Barbu, Multiscale modelling of defect kinetics in irradiated iron, Nat. Mater. 4 (2005) 68–74, http://dx.doi.org/10.1038/nmat1286.
[16] R.E. Stoller, M.B. Toloczko, G.S. Was, A.G. Certain, S. Dwaraknath, F.A. Garner, On the use of SRIM for computing radiation damage exposure, Nucl. Instrum. Methods Phys. Res. Sect. B Beam Interact. Mater. At. 310 (2013) 75–80, http://dx.doi.org/10.1016/j.nimb.2013.05.008.
[17] M.G. Horsten, M.I. de Vries, Tensile properties of type 316L(N) stainless steel irradiated to 10 displacements per atom, J. Nucl. Mater. 212 (1994) 514–518, http://dx.doi.org/10.1016/0022-3115(94)90114-7.
[18] Material Reliability Program, Development of Material Constitutive Model for IrradiatedAustenitic Stainless Steels (MRP-135-Rev. 1), EPRI, Palo Alto, CA, 2010, 1020958.
[19] C. Pokor, Y. Brechet, P. Dubuisson, J.-P. Massoud, X. Averty, Irradiation damage in 304 and 316 stainless steels: experimental investigation and modeling. Part II: irradiation induced hardening, J. Nucl. Mater. 326 (2004) 30–37, http://dx.doi.org/10.1016/j.jnucmat.2003.12.008.
[20] R.E. Schramm, R.P. Reed, Stacking fault energies of seven commercial austenitic stainless steels, Metall. Trans. A 6 (1975) 1345, http://dx.doi.org/10.1007/BF02641927.
[21] C. Sun, S. Zheng, C.C. Wei, Y. Wu, L. Shao, Y. Yang, K.T. Hartwig, S.A. Maloy, S.J. Zinkle, T.R. Allen, H. Wang, X. Zhang, Superior radiation-resistant nano-engineered austenitic 304L stainless steel for applications in extreme radiation environments, Sci. Rep. 5 (2015) 7801, http://dx.doi.org/10.1038/srep07801.
[22] L. Vitos, A.V. Ruban, H.L. Skriver, J. Kollár, The surface energy of metals, Surf. Sci. 411 (1998) 186–202, http://dx.doi.org/10.1016/S0039-6028(98)00363-X.
[23] Z. Jiao, G.S. Was, Impact of localized deformation on IASCC in austenitic stainless steels, J. Nucl. Mater. 408 (2011) 246–256, http://dx.doi.org/10.1016/j.jnucmat.2010.10.087.
[24] S. Bruemmer, et al., Characterization of Neutron-Irradiated 300-Series Stainless Steels to Assess Mechanisms of Irradiation Assisted Stress Corrosion Cracking, Final Report, EPRI Project WO4068–20, November 2000.
[25] M. Toloczko, G. Lucas, G. Odette, R. Stoller, M. Hamilton, An investigation of microstructures and yield strengths in irradiated austenitic stainless steels using small specimen techniques, in: D. Gelles, R. Nanstad, A. Kumar, E. Little (Eds.), Eff. Radiat. Mater. 17th Int. Symp., ASTM International, 100 Barr Harbor Drive, PO Box C700, West Conshohocken, PA 19428-2959, 1996, 902–902–17, http://www.astm.org/doiLink.cgi?STP16515S (accessed December 17, 2016).
[26] A.C. Fischer-Cripps, Nanoindentation, Springer New York, New York, NY, 2004. http://link.springer.com/10.1007/978-1-4757-5943-3 (accessed August 2, 2016).